Spatial genome organization in nematodes with programmed DNA elimination

James R. Simmons[1], Tianchun Xue[2], Rachel Patton McCord[1,2], Jianbin Wang[1,2,#]

[1] Department of Biochemistry and Cellular and Molecular Biology, University of Tennessee, Knoxville, TN 37996, USA

[2] UT-ORNL Graduate School of Genome Science and Technology, University of Tennessee, Knoxville, TN 37996, USA

Corresponding author, jianbin.wang@utk.edu

Abstract

Programmed DNA elimination (PDE) is a notable exception to genome integrity. In many nematodes, PDE is initiated by DNA double-strand breaks (DSBs), leading to chromosome fragmentation and subsequent DNA loss. However, the mechanism of nematode programmed DNA breakage remains largely unclear. In the human and pig parasitic nematode *Ascaris* (*A. lumbricoides* and *A. suum*), no conserved motif or sequence structures are present at chromosomal breakage regions (CBRs), suggesting the recognition of CBRs may be sequence-independent. Using Hi-C, we reveal that *Ascaris* CBRs engage in three-dimensional (3D) interactions before and during PDE, indicating that physical contacts between break regions may contribute to PDE. The 3D interactions are established in both *Ascaris* male and female germlines, demonstrating inherent genome organization associated with the CBRs and to-be-eliminated sequences. In contrast, in the unichromosomal horse parasite *Parascaris univalens*, transient pairwise interactions between neighboring CBRs that will form the ends of future somatic chromosomes are observed only during PDE. We find that *Ascaris* PDE, which converts 24 germline chromosomes into 36 somatic ones, induces specific compartmentalization changes. *Parascaris* PDE generates the same set of 36 somatic chromosomes, and the 3D compartment changes following PDE are consistent between the two species. Overall, we suggest that CBRs are associated with the boundaries of distinct 3D

genome domains. These domains partition the retained and eliminated DNA into separate spatial compartments. We also demonstrate that following PDE, the 3D genome reorganization of the somatic chromosomes in these nematodes is evolutionarily and developmentally conserved.

Keywords

Programmed DNA elimination (PDE); DNA double-strand breaks (DSBs); chromosomal breakage regions (CBRs); Hi-C; 3D genome organization; *Ascaris*; *Parascaris*; nematode; chromosome compartment; karyotype.

Introduction

Genome integrity is crucial for faithful inheritance of genetic material. However, during the development of many species, programmed DNA elimination (PDE) removes a substantial portion of the genome, leaving daughter cells with reduced DNA content (Wang and Davis 2014; Dedukh and Krasikova 2021; Zagoskin and Wang 2021; Drotos et al. 2022; Kloc et al. 2022; Mochizuki 2024). Although PDE is not present in most traditional model organisms with the exception of ciliates, it is being identified in a growing number of species from diverse phyla (Grishanin 2014; Streit et al. 2016; Rzeszutek et al. 2020; Smith et al. 2021; Borodin et al. 2022; Chen et al. 2022; Estrem and Wang 2023; Herbette and Ross 2023). While PDE is gaining increasing recognition as a significant biological process (Bendich and Rogers 2025; Hanlon et al. 2025), much remains unknown about its molecular mechanisms, particularly in metazoan species that exhibit PDE.

DNA double-strand breaks (DSBs) fragment chromosomes during PDE in ciliates, many nematodes, and some copepods (Wang and Davis 2014; Zagoskin and Wang 2021; Mochizuki

2024). In these species, specific genomic locations are recognized, DSBs are generated, DNA break ends are healed by telomere addition or end joining, and specific regions of the genome are retained or eliminated. Although the molecular machineries for PDE appear divergent between the ciliates and nematode systems, both sequence-dependent and sequence-independent mechanisms are used for break site recognition (Betermier et al. 2023; Estrem and Wang 2023; Mochizuki 2024; Srinivasan et al. 2026). DSBs in the middle of the germline chromosomes, if healed with telomere addition, can lead to the partitioning of the chromosomes and drastic changes in the resulting somatic karyotypes (Simmons et al. 2024). However, the consequences of these karyotype changes on genome organization and gene expression are largely unexplored.

The parasitic nematodes infecting human (*A. lumbricoides*) and pig (*A. suum*) undergo PDE (Wang and Davis 2020; Estrem and Wang 2023). The two species have little difference in genome sequences (Easton et al. 2020) and PDE. For simplicity, we use *Ascaris* to refer to both species. In *Ascaris*, we identified 72 chromosomal breakage regions (CBRs) at the boundaries of retained and eliminated DNA, with 48 terminal CBRs located near the chromosome ends and 24 internal CBRs in the middle of the chromosomes (Wang et al. 2020). Each CBR is in a 3-6 kb window where DSBs occur and new somatic telomere sequences are added to repair the broken ends (Wang et al. 2017; Wang et al. 2020). Sequence analysis revealed no conserved motifs or sequence structures at these CBRs, suggesting a sequence-independent mechanism for their recognition (Estrem and Wang 2023). Moreover, common histone marks and small RNAs are not associated with the CBRs (Zagoskin et al. 2025). However, the chromatin at the CBRs becomes more accessible during PDE, indicating a specific mechanism may be involved (Wang et al. 2017; Wang et al. 2020). Similarly, the horse parasite *Parascaris univalens* also undergoes PDE, but its germline karyotype is a single, large chromosome (~2.5 Gb), of which ~2.2 Gb of repetitive heterochromatin is confined to the arms and eliminated during PDE

(Simmons et al. 2024). In contrast to *Ascaris*, the 72 CBRs in *Parascaris* are all internal, ~1 Gb away from either chromosome end (Simmons et al. 2024).

The lack of sequence features associated with *Ascaris* and *Parascaris* CBRs prompted the search for sequence-independent mechanisms that might be involved in PDE. The eukaryotic genome is organized at a 3D level into folded structures at multiple length scales, involving both intrachromosomal and interchromosomal interactions (McCord et al. 2020; Dekker and Mirny 2024). Changes in 3D genome organization have been implicated in numerous developmental processes, such as V(D)J and class switch recombination in lymphocytes (Zhang et al. 2012; Hu et al. 2015), zygotic genome activation during embryogenesis (Gassler et al. 2017; Kaaij et al. 2018), X-chromosome inactivation in mammals (Minajigi et al. 2015; Giorgetti et al. 2016), dosage compensation in *C. elegans* (Crane et al. 2015), antigenic variation and transcription in trypanosomes (Muller et al. 2018; Rabuffo et al. 2024), and neural development (Bonev et al. 2017; Rajarajan et al. 2018). We hypothesize that the 3D genome architecture may contribute to PDE by spatially organizing 1) the CBRs before and during PDE and 2) the resulting somatic chromosomes after PDE. Notably, in *Ascaris*, introducing random DSBs by treating with X-rays at PDE embryo stages did not lead to their repair through telomere addition (Estrem et al. 2024). One possibility is that recruitment of telomere addition machinery to *Ascaris* PDE break sites requires the nuclease responsible for generating the DSBs. This further suggests that these DSBs and the telomere healing process are specific and may be confined within nuclear foci where the machineries for PDE could localize.

Recent advancements in chromosome conformation capture (Hi-C) have unveiled major principles of 3D genome organization, encompassing chromosome territories, compartments, topologically associating domains, point interactions, and acting through mechanisms such as phase separation and loop extrusion (Goloborodko et al. 2016; Strom et al. 2017; Zheng and

Xie 2019; McCord et al. 2020; Feric and Misteli 2021; Dekker and Mirny 2024; Li et al. 2024). Here, we used Hi-C across embryonic stages before, during, and after PDE in *Ascaris* and *Parascaris* to determine whether CBRs engage in 3D interactions, how the 3D genome reorganizes following elimination, and whether these features are conserved between the two species.

Results

Chromosomal breakage regions interact with each other during *Ascaris* DNA elimination

Ascaris early embryogenesis is slow (~15 hours per cell cycle) and synchronous, allowing collection of large quantities of embryos from discrete developmental stages (Wang and Davis 2020). This provides a unique opportunity to study the PDE process (Figure 1A), which occurs during the 4-16-cell embryonic stages (Estrem and Wang 2023). The high degree of synchrony (Azzaria and McGhee 1992) ensures that embryos collected at each timepoint are predominantly (>85%) at the indicated stage (Wang et al. 2014; Wang and Davis 2020). We performed Hi-C on *Ascaris* embryos at stages before (2-4 cells; 48 hr), during (4-8 cells; 60 hr), and after (32-64 cells; 5 days) PDE. The Hi-C data were mapped to an improved germline genome assembly that corrects previous mis-assemblies (see Supplemental Fig. S1). The Hi-C heatmaps confirm the splitting of a single germline chromosome into multiple somatic chromosomes (Figure 1B). Across the genome, the Hi-C maps revealed a pattern of interactions prior to and during PDE among chromosome ends where the 48 CBRs reside (Figure 1C and 1E, black arrows). These interactions are not due to mapping artifacts caused by repetitive sequences, since mapping the Hi-C data to a repeat-masked genome still produced the same pattern of interactions (Supplemental Fig. S2). The interactions are significantly higher than expected based on their genomic distance (Supplemental Fig. S3). Interactions also occur among the 24 internal CBRs (Figure 1C and 1E, green arrows). The terminal and internal CBRs form two spatially separated groups (Figure 1D and 1F). The two groups showed distinct

interaction patterns, with terminal CBRs forming either discrete point or streak interactions, while internal CBR interactions appeared as long streaks (Figure 1G). Notably, these interactions, largely associated with the retained DNA (see Figure 3), disappear after PDE, consistent with the timing of DNA elimination (Figure 1). Since the CBR is a unique feature associated with PDE, our data established a strong link between CBR 3D interactions and PDE.

CBR interactions are established during germline development

We next asked when the CBR interactions are formed during development. We performed Hi-C on male and female germline tissues and on 1-cell zygotes (0 hr), stages not associated with PDE. We found that interactions among CBRs were already present in these germline tissues (Figure 2). Thus, these long-range CBR interactions are established well before PDE and may be an intrinsic feature associated with the CBRs and germline chromosomes. The patterns of 3D interactions at the ends of chromosomes exhibited variations among these stages (Figure 2). In the testis and 1-cell zygote, the ends of certain chromosomes are observed to interact with the entire length of many other chromosomes, resulting in stripes in the Hi-C maps (Figure 2A and 2C). In contrast, in the ovary, most interactions are more confined to the ends of the chromosomes, as indicated by the dots in the Hi-C maps (Figure 2B). Even though there is a small fraction (5-10%) of somatic cells in the testis and ovary samples (Wang et al. 2012), we reason the stripe and dot patterns observed are unlikely due to somatic contamination, because they are also present in the 1-cell zygote which is free of somatic cells. Overall, while our data demonstrate a consistency in the CBR interactions throughout germline development, they also reveal stage-specific variations.

CBRs reside at the boundaries of the spatially organized chromosome ends

To identify the precise spatial boundaries of the CBR interactions among chromosomes, we determined *trans*-interaction (interchromosomal) frequencies surrounding the CBRs. We chose

to examine interchromosomal interactions of all assembled terminal CBRs using 100 kb in the eliminated regions and 500 kb in the retained regions (Figure 3A; total 45 out of 48 terminal CBRs). This analysis revealed a significant enrichment of *trans* interactions within ~200 kb of retained DNA adjacent to the terminal CBRs (Figure 3A). CBRs coincide with the boundaries of the high and low interchromosomal interaction regions (Figure 3A, vertical line), suggesting these strong interactions may spatially demarcate the retained and eliminated sides of the DNA. This spatial separation is not detected for internal CBRs (Supplemental Fig. S4), indicating that the stronger interchromosomal interactions for terminal CBRs are associated with their proximity to the chromosome ends. Notably, a steep drop in trans interactions is observed at ~300 kb of the retained region (Figure 3A), indicating the possible boundary of the spatially organized domain.

To further distinguish whether the elevated interchromosomal interactions in the CBR-flanking regions were driven by a few selected chromosomes or across all chromosomes, we analyzed the contribution of individual chromosomes. Each chromosome contributed considerably to the aggregated interactions (Figure 3B), suggesting a shared mechanism of 3D genome organization among these chromosomes. These interactions for CBR-adjacent retained regions are dynamic during embryo development, with the highest interactions observed in the early embryos; they gradually decrease throughout embryonic development and become minimal after PDE at 32-64-cell embryos (Figure 3A). Collectively, these results indicate that the chromatin architecture associated with CBRs employs long-range *trans* interactions prior to PDE. These interactions may play a key role in defining the boundaries of 3D genome domains that coincide with the CBRs, thus spatially separating the retained and eliminated DNA.

Short-range interactions and 3D insulation associated with PDE

To explore whether short-range 3D interactions might also influence PDE, we calculated insulation scores across the genome. Insulation scores quantify the degree to which a given region interacts with its local genomic neighborhood. For Hi-C insulation scores, lower numbers indicate stronger insulation while higher numbers denote weaker insulation. Thus, dips in insulation score are interpreted as stronger local boundaries across which fewer interactions occur (Crane et al. 2015; Lajoie et al. 2015). We identified many genomic regions with dynamic insulation patterns during development (Figure 3C-D). Notably, out of the 44 completely assembled eliminated regions exceeding 100 kb that allow robust insulation analysis, 35 (80%) consistently exhibited boundary-like dips in insulation score at or near their respective CBRs before PDE, suggesting strong local boundaries at the CBRs. Six other CBRs (Chr 5a, Chr 9, Chr 10, Chr 12b, Chr 19, Chr X2b; 14%) demonstrated similar drops in insulation score in adjacent retained regions (Supplemental Fig. S5) and only one eliminated region (Chr X5) did not show any sign of boundary-like insulation.

After PDE, the retained regions adjacent to CBRs become less insulated as indicated by the increasingly positive insulation scores, extending beyond 1 Mb (Figure 3C-D). The new chromosome ends also exhibit decreased gene expression, despite showing higher chromatin accessibility measured by ATAC-seq (Wang et al. 2017). Consistently, the heterochromatic histone mark H3K9me3 accumulates at the new chromosome ends after PDE (Supplemental Fig. S6). We observed a general decrease in insulation across eliminated regions up to their elimination (Figure 3D). This coincided with the incorporation of the eliminated DNA fragments into micronuclei (Wang et al. 2020) which separate these fragments from the rest of the genome, thus may increase their local interactions.

Overall, the chromosomal-level 3D and short-range interactions of CBRs may play a role in the PDE process by bringing them to nuclear foci that may have accumulated molecular machinery

essential for DSBs and telomere addition (PDE foci; see Figure 3E and discussion). Alternatively, the interactions of the CBRs themselves may act as a platform to recruit CBR- and/or PDE-associated proteins to the break sites.

3D chromosomal changes following programmed DSBs for PDE

The generation of DSBs and new chromosome ends through PDE also leads to 3D genome changes. To study the local insulation in response to the DSBs, we performed Hi-C analysis on several staged embryos post-PDE (Figure 4) and determined the insulation scores specifically for CBRs. Because the eliminated DNA is no longer available in the genomes of post-PDE stages, we only examined the retained region within 100 kb sequences around CBRs. These regions became more insulated from the 1-cell zygote to PDE stage (4-8 cells) but became less insulated after PDE (32-64 cells) (Figure 4A). This suggests that DSBs may liberate the spatial constraints adjacent to the CBRs during PDE, thus changing their local genomic contacts. Overall, this analysis revealed a consistent pattern of local 3D genome in response to DSBs post-PDE.

Long-range interaction changes and chromosome clustering through PDE

To assess the impact of PDE on intrachromosomal contacts, we analyzed distance decay curves across different stages (Figure 4B). In the 1-cell zygote, interaction frequency exhibits a power-law decay diminishing around 23 Mb, which aligns with the largest germline chromosome size (Chr X1 = 23.1 Mb). Short-range interactions (<100 kb) increase after PDE, coinciding with the observed increase in local structures (Figure 1C, 32-64 cell). This suggests the establishment of short-range regulatory interactions throughout the genome following PDE. Conversely, long-range interactions (>1 Mb) decrease after PDE, consistent with the overall reduced chromosome sizes (average size: germline = 12.8 Mb and soma = 7 Mb).

To determine how the genome spatially reorganizes at chromosomal level following PDE, we clustered chromosomes at each developmental stage based on Hi-C contact frequencies. In the 1-cell zygote and 2-4-cell embryos, interactions among pre-PDE chromosomes are uniform (Figure 4C). After PDE, the somatic chromosomes exhibit differential spatial organization. A key feature after PDE is the clustering of sex chromosomes: at 32-64 cells, the 9 sex chromosomes form a distinct group separated from the 27 autosomes. This segregation of the sex chromosomes becomes more pronounced in larvae L1 (except for Chr X4a). In contrast, for autosomes, they are organized into several large, distinct clusters, indicating progressive establishment of preferential interactions between chromosome territories (Figure 4C). These data suggest coordinated compartmentalization changes (see also Figure 5) may contribute to the formation of the somatic chromosome territories after PDE.

Karyotype changes during PDE are associated with compartmental and somatic 3D genome reorganization

Ascaris PDE leads to extensive karyotype changes and the splitting of 11 of the 24 germline chromosomes into 23 of the 36 somatic chromosomes (Wang et al. 2020). In *C. elegans*, Hi-C compartments exhibit a general profile for autosomes, where the active (A) compartments are in the middle of the chromosomes and inactive (B) compartments are in the arms of the chromosomes, forming a linear B-A-B profile along its arm-center-arm (Sawh and Mango 2022). This B-A-B profile is consistent with expression data that more conserved and active genes are located in the middle of the chromosomes (Gerstein et al. 2010).

To investigate whether and how large-scale chromosomal contact domains change after *Ascaris* PDE, we first determined the A/B compartmentalization pattern using the first eigenvector (PC1) of the Hi-C data (Figure 5A and Supplemental Fig. S7). We validated these compartments as transcriptionally active and inactive, respectively, using independent and comprehensive multi-

omics datasets from previous studies (Wang et al. 2014; Kang et al. 2016; Wang et al. 2017; Wang et al. 2020) (Figure 5B). Analysis of strongly compartmentalized regions (defined as EV1 > 0.15 or < -0.15) revealed that active chromatin marks, including H3K4me3, H3S10P, H3K36me2, and H3K36me3, are significantly enriched in A compartments. Conversely, H3K9me3, a marker of repressive chromatin, is significantly enriched in B compartments (Figure 5B). Furthermore, RNA-seq, RNA Polymerase II, and ATAC-seq analyses also show significantly higher signal in A compartments, corroborating the compartment data (Figure 5B).

Ascaris 3D genome compartmentalization is weak during early development, up to the embryonic stages of PDE (4-8 cells), after which compartments are strengthened (Figure 5A and Supplemental Fig. S8A). This strengthening of compartments overall reflects both large-scale changes in karyotype, due to the increased number of chromosomes following PDE, and smaller-scale chromatin reorganization typical of early embryogenesis in nematodes (Sawh et al. 2020; Jash and Csankovszki 2024). We observed notable compartmentalization changes surrounding the CBRs before and after PDE. Prior to PDE, the eliminated regions exhibit opposite compartments relative to retained regions. After PDE, somatic chromosomes adopted distinct patterns of A/B compartmentalization (Figure 5A and 5D). Genome-wide analysis revealed that in the 32-64-cell embryos, a stage immediately following PDE, the Hi-C compartments exhibit the most variable structure (Figure 5A). This coincides with a significant drop in saddle strength that measures the degree of separation between active and inactive compartments (Figure 5C and Supplemental Fig. S8B). Our data suggest that the 32-64-cell stage is likely a transition phase for compartmentalization, where future somatic compartments are not fully established. This transition is further demonstrated by the compartment identity switching (A-to-B and B-to-A): it is stable before PDE (1-cell; Supplemental Fig. S8C) but shows a significant increase in A-to-B switching at 32-64-cell embryos and more B-to-A switching between the 32-64-cell and L1 stages. Notably, compartmentalization changes for the somatic

chromosomes are stabilized at the L1 stage where the somatic program is firmly established (Figure 5A and 5D). Overall, our findings indicate that the karyotype changes accompanying *Ascaris* PDE are associated with distinct reorganization of the 3D genome in somatic cells.

CBRs in *Parascaris* form transient and pairwise interactions during PDE

The related horse parasite *Parascaris* undergoes PDE during 2-32 cell embryonic stages (Estrem and Wang 2023; Simmons et al. 2024). To determine if the CBRs in *Parascaris* also form 3D genome interactions, we performed Hi-C in embryos before (1 cell; 10 hr), during (2-4 cells; 17 hr), and after PDE (4-8 cells; 24 hr). The synchrony of the *Parascaris* early development is less consistent compared to *Ascaris*, but at each timepoint, >70% of the embryos are at the indicated stage. Since the ~2.2 Gb of terminal heterochromatin arms are exclusively satellite repeats and are not present in the genome assembly, the Hi-C map spans only the euchromatic core. Nevertheless, all 72 CBRs are included in the one assembled chromosome. In 1-cell embryos before PDE, the whole chromosome is largely unstructured at the 3D genome level (Figure 6A and Supplemental Fig. S9). However, in the 2-4-cell stage, where PDE begins, we observed a striking pattern of CBR interactions: neighboring pairs of CBRs that will form the ends of future somatic chromosomes interact with each other (Figure 6A-B). We refer to the two CBRs flanking a single retained segment - those that will form the two ends of the same somatic chromosome - as a cognate CBR pair; CBRs belonging to different prospective somatic chromosomes are referred to as non-cognate. When the Hi-C contact frequencies were normalized by the expected pattern of distance decay, 36 sites of higher-than-expected interactions became apparent (Figure 6B-D). The sites of interactions match the ends of the 36 future somatic chromosomes (36 cognate CBR pairs).

Like *Ascaris*, these *Parascaris* CBR interactions are formed within retained sequence and peak at the boundaries of the retained and eliminated DNA (Figure 6E). The interaction is highly

specific to cognate CBRs rather than a general increase in contact near CBRs (Supplemental Fig. S10A). Quantified per chromosome, cognate CBR interactions rose from a median observed/expected (O/E) ratio of 0.20 before PDE to 0.55 O/E during PDE — an increase seen in all 33 chromosomes tested ($P = 2.3 \times 10^{-10}$). The median interactions O/E fell to 0.35 after PDE ($P = 2.1 \times 10^{-7}$; Supplemental Fig. S10B–C). Interaction strength was not related to somatic chromosome length or the size of the adjacent eliminated block, nor did it differ in the autosome vs. sex chromosome regions of the germline chromosome (Supplemental Fig. S10D). Stronger interactions are observed in cognate CBR pairs regardless of their separation along the germline chromosome, whereas weaker non-cognate interactions are detected but are restricted to CBR pairs within ~50 Mb of each other (Figure 6B–C). This contrasts with the nearly all-to-all trans interactions among *Ascaris* chromosome ends prior to PDE (Figure 1C–D). Overall, these data show that specific, transient 3D CBR interactions occur only during PDE, suggesting a role for pairwise CBR interactions in *Parascaris* PDE (Figure 6F).

Conserved compartment structure in *Ascaris* and *Parascaris* supports a role for PDE in somatic nuclear reorganization

Previous comparative analyses have shown that at sequence level, *Ascaris* and *Parascaris* have the same set of somatic chromosomes after PDE (Simmons et al. 2024). To determine if similar programmed compartmentalization changes also occur in *Parascaris* at the 3D genome level, we performed Hi-C on matching embryonic stages in *Parascaris*. Analysis of the compartments in both nematodes showed a strong correlation between the two species in post-PDE stages (Figure 7A). The majority of the matching somatic chromosome pairs (30/36; 83%) have a positive correlation coefficient of the eigenvector value ranging from 0.19 to 0.95 (median = 0.49) (Figure 7A). Importantly, for many matching pairs, such as Chr01a/Chr05, Chr06b/Chr07, Chr02a/Chr16, and Chr14/Chr21, the somatic compartment patterns are mirrored in *Ascaris* and *Parascaris* (Figure 7A). Considering the divergence of the two species

(Qing et al. 2025) and the sampling variations, the similarity of the Hi-C compartments is highly significant. Overall, our result suggests that PDE not only generates the same somatic chromosomes in these two parasites, but the resulting chromosomes undergo the same programmed compartmental changes after PDE, indicating a conserved somatic 3D genome after PDE.

Discussion

In the nematode ascarids, DSBs occur within the CBRs of the germline genome, initiating PDE (Figure 1A). This process results in a highly reduced somatic genome. However, the mechanistic understanding of this process remains elusive. Here, using discrete staged embryos, we carried out Hi-C to examine the 3D genome organization before, during, and after PDE in both *Ascaris* and *Parascaris*. Two major findings emerged from our analyses (summarized in Figure 7B). First, strong 3D genome interactions among the CBRs are associated with PDE, indicating the 3D genome may facilitate the break site recognition, DSB generation or DNA repair. Second, PDE is associated with substantial and conserved compartmentalization changes in the somatic chromosomes of both nematodes, suggesting that by removing the 3D genome constraints (eliminated DNA), PDE could play a critical role in reorganizing the somatic 3D genomes.

Recognition of CBRs and organization of PDE foci through 3D genome organization

Ascaris CBRs interact with each other prior to and during PDE (Figure 1). These interactions extend beyond the sites of CBRs, often covering the neighboring ~200 kb of retained genome regions (Figure 3). Notably, many CBRs are located at the boundary of the spatially organized chromosome ends (Figure 3A), and significant insulation is observed in eliminated regions prior to elimination (Figure 3C). These findings suggest that CBRs are unique within *Ascaris*'s 3D genome organization and spatially demarcate the retained and eliminated sides of the DNA.

Previous molecular data suggest CBR recognition is likely not dependent on specific sequences (Wang et al. 2017; Wang et al. 2020). Our Hi-C results lead us to propose a model for a sequence-independent mechanism of CBR recognition during *Ascaris* PDE (Figure 3E and Figure 7B). We hypothesize that CBRs interact with each other at foci where the machinery for DNA breaks and telomere healing is concentrated (PDE focus; Figure 3E and Figure 7B). The model is consistent with the population-level Hi-C interactions observed during PDE. The model is also consistent with a mechanism that does not require nucleotide precision to generate DSBs (Estrem et al. 2024), although it is plausible that other attributes of the CBRs and their localization could enhance the formation and function of PDE foci.

Chromosome end interactions that form the telomere bouquet are a common form of 3D chromosome organization during meiosis (Harper et al. 2004; Tomita and Cooper 2007; Tsai and McKee 2011; Blokhina et al. 2019; Thadani et al. 2026). However, the interactions we observed at chromosome ends are unlikely caused by the telomere interactions. This is because the terminal CBRs have significantly higher trans chromosomal interactions at the retained sides of breaks, which are farther away from telomeres compared to the eliminated sides (Figure 3). It remains to be determined if specific sequences within the retained DNA are associated with these interactions. Furthermore, we noticed that internal CBRs, which are far away from telomeres, also exhibit similar types of interactions (Figure 1B-C). Consequently, we believe that the interactions observed at chromosome ends are likely unique to CBRs but not linked to telomeres. However, due to their locations near the ends of the chromosomes, we currently cannot determine whether the dynamic changes of interactions at the ends are caused by CBRs, telomeres, or both. Notably, we achieved a very high resolution of our Hi-C data by using multiple restriction digestions and high sequencing depth (for instance, 5 kb for Figure 3). Using these high-resolution Hi-C maps, we did not identify any other significant long-range or interchromosomal pairwise interactions across the genomes (Figures 1, 2, 6). Thus, the CBR

interactions stand out as a unique feature of the 3D genome in these nematodes, setting it apart from any other nematode species examined so far (Crane et al. 2015; Bian et al. 2020; Kim et al. 2022; Das et al. 2024; Kim et al. 2025). The CBRs are the sites where DNA breaks occur, and evolutionarily, they are functionally conserved in both *Ascaris* and *Parascaris*. This highlights the significance of these interactions in PDE species.

A plausible mechanism for organizing the PDE foci is through phase-separated condensates (Hyman et al. 2014; Shin and Brangwynne 2017; Sabari et al. 2020; Feric and Misteli 2021; Fujishiro et al. 2025). In other systems, such as olfactory receptor clustering in mammalian cells, phase-separated condensates can reinforce strong interchromosomal interactions similar to the ones observed between CBRs (Pulupa et al. 2025). We suggest proteins and RNAs involved in DNA breaks and telomere addition may concentrate in PDE foci during DNA elimination. Recent studies on the ssDNA-binding protein RPA (Spegg et al. 2023) and telomeres and shelterin components (Jack et al. 2022; Soranno et al. 2022) suggest they could also contribute to the formation of dynamic liquid-like droplets. Furthermore, there is precedence for co-localization of chromatin regions at sites enriched for processing enzymes such as RNA splicing and nuclear speckles (Giudice and Jiang 2024). Additional factors, such as sequence- or nucleosome-dependent elements, may further contribute to the positioning of the CBRs for foci formation and DSB generation. Overall, our data suggest that the CBRs represent a unique genomic feature in nematode PDE at the boundary between the retained and eliminated DNA, and the 3D genome organization of the CBRs and chromosome ends may contribute to their recognition, foci formation, and the initiation and/or execution of PDE.

In *Ascaris*, the CBR and chromosome end interactions precede PDE in the germline and early embryos (Figure 2). It remains to be determined whether these interactions persist through fertilization and pronuclear fusion or if they are erased and re-established in the zygote. Even

414 though these interactions exist in the germline, the factors associated with PDE foci (Figure 3E)
415 formation and function may not be present, thereby preventing PDE from occurring in germline.
416 We speculate that these interactions in germline stages serve a separate germline function,
417 likely involved in chromosome organization during meiosis (Thadani et al. 2026). In *C. elegans*,
418 pairing and synapsis are achieved through the recognition of the pairing centers at one end of
419 each chromosome by four related zinc finger proteins (MacQueen et al. 2005; Phillips and
420 Dernburg 2006). These zinc-finger pairing-center proteins and many other genes involved in *C.*
421 *elegans* homolog pairing are absent in *Ascaris* and *Parascaris* (Simmons et al. 2024). Because
422 these pairing-center proteins appear restricted to *Caenorhabditis* and its close relatives, their
423 absence in *Ascaris* and *Parascaris* most likely reflects their origin within the *Caenorhabditis*
424 lineage rather than a loss associated with PDE (Simmons et al. 2024; Stevens et al. 2025).
425 These ascarid species must therefore pair their homologs by other means. Our Hi-C data
426 provide support that indeed, these germline chromosomes can interact with each other using
427 their chromosome ends (Figure 2). These interactions may be an intrinsic feature associated
428 with the sequences at the chromosome ends. During PDE, these sequences are removed, and
429 the interactions among retained regions near the CBRs are abrogated. Therefore, PDE may
430 offer a means to remove chromosome ends that function in the germline but are no longer
431 required or may even be harmful in somatic cells. Some of these CBRs show interactions along
432 the entire length of multiple other chromosomes, leading to the formation of long stripe patterns
433 in the Hi-C map (Figures 1 and 2). These long stripes could potentially signify an active
434 searching, scanning, or looping mechanism.
435
436 The CBRs from *Parascaris* also interact during PDE. However, unlike *Ascaris* CBRs that form
437 extensive interactions among the two CBR groups (Figure 1B), *Parascaris* CBRs engage in
438 pairwise interactions mostly for cognate CBR pairs from the future ends of each somatic
439 chromosome (Figure 6). The *Parascaris* pairwise CBR interactions are weaker than *Ascaris*

CBR interactions and occur transiently only during PDE stages. They are reminiscent of the "beads-on-a-string" model proposed based on an early cytology study (Niedermaier and Moritz 2000), where the "beads" represent retained and condensed future somatic chromosomes, whereas the "string" represents internally eliminated DNA associated with more loose chromatin during PDE (Figure 6F). Thus, our Hi-C data appear to corroborate the cytologic observation that the CBRs in *Parascaris* are at the boundaries of spatially organized chromosomes that could separate the retained and eliminated DNA (Figure 6). The differences in CBR interactions observed in these two nematodes may be attributed to the unique organization of the single homologous pair of the 2.5-Gb *Parascaris* germline chromosomes (Simmons et al. 2024). *Ascaris* CBRs are distributed across 24 chromosomes that can interact more freely in the nucleus, whereas all 72 *Parascaris* CBRs are confined to a single 240-Mb euchromatic core flanked by heterochromatic arms comprising >85% of the genome. The distribution of CBRs in *Parascaris* constrains their 3D interactions, consistent with our observation that interactions are limited to CBRs within ~50 Mb of each other (Figure 6C).

PDE provides a means to reorganize the somatic chromosomes

PDE resolves fused germline chromosomes (*Ascaris* = 24 and *Parascaris* = 1) into the same set of 36 somatic chromosomes (Simmons et al. 2024) (Figure 7B). We previously suggested that the restoration of the somatic karyotype may confer biological functions (Simmons et al. 2024). Here, we demonstrate that the somatic 3D genome organization, as exemplified by the compartmentalization changes following PDE, is conserved between the two species (Figure 7A). While the impact of these compartmentalization changes on individual genes may be limited or negligible, the aggregate effect on numerous genes influenced by these changes could be substantial. Although the evolutionary trajectories leading to the current germline chromosomes are different (Simmons et al. 2024), partitioning of the germline chromosomes leads to somatic chromosomes that retain the "memory" of the ancestral 3D genome

organization. This underscores the important role of PDE in splitting the fused germline chromosomes.

Chromosome reorganization is a common response to DSBs (Sanders et al. 2020; Arnould et al. 2023; Zagelbaum et al. 2023; Chiolo et al. 2025). Unlike most DSBs that are repaired using non-homologous end joining or homologous recombination, DSBs induced by PDE in nematodes are healed through telomere addition (Muller et al. 1991; Estrem et al. 2024). This telomere-mediated repair process may also contribute to chromosome reorganization by forming condensates surrounding the break sites. Analysis of the Hi-C data across all 36 somatic chromosomes revealed consistent temporal changes in the 3D genome structure, showing the decreased insulation at and around the DSBs during PDE (Figure 4A). This change may be attributed to 1) the liberation of CBRs from their germline chromosome locations, 2) the DSB and telomere healing mechanisms, and 3) the formation of new heterochromatic regions at the somatic chromosome ends.

In the ciliate *Tetrahymena thermophila*, distinct higher-order chromatin organization were observed in the germline micronucleus and somatic macronucleus (Luo et al. 2020), suggesting that the 3D genome may play important roles during the development of the macronucleus chromosomes during PDE. Similarly, a recent study in the ciliate *Oxytricha trifallax* also suggested widespread 3D genome reorganization before the onset of PDE (Villano et al. 2025). Another recent genomic study in the ciliate *Paramecium aurelia* found that the ends of the germline chromosomes form a distinct genomic compartment that is eliminated during early somatic development (Arnaiz et al. 2026). These ciliate findings echo the spatial separation of retained and eliminated DNA that we observe at the 3D level in nematodes (Figure 3).

The B-A-B compartment profile of *C. elegans* chromosomes may be associated with the ancestral linkage groups in nematodes known as Nigon elements (Tandonnet et al. 2019; Gonzalez de la Rosa et al. 2021). Recent studies show that fused chromosomes retain the centrality of the active compartment (Yoshida et al. 2023; Chung et al. 2026). However, this compartment profile is not consistently observed in *Ascaris* and *Parascaris* somatic chromosomes, even though Nigon elements are largely maintained in their genomes (Simmons et al. 2024). Some of these differences could be attributed to the more discrete early embryo stages used in our study, although Hi-C data from a strictly somatic tissue (such as the intestine (Simmons et al. 2024)) also did not exhibit a consistent B-A-B compartment profile. Since *Ascaris* and *Parascaris* belong to the distant clade III of nematodes, it is plausible that their compartment profiles may have diverged from those of rhabditid nematodes (clade V), where Nigon elements were originally defined. Although many of the observed compartmental changes are specifically linked to the break sites associated with PDE (Figures 5 and 7A), we recognize that PDE occurs alongside other dynamic developmental processes during embryogenesis, thus it is also plausible that some of these compartmental changes may be part of the developmental program.

Together, our findings integrate PDE into the broader framework of nematode chromatin organization. In these ascarids, the 3D genome spatially demarcates the retained and eliminated DNA before PDE. Following PDE, the 3D genome adopts a conserved somatic organization, suggesting that genome architecture is both a contributor to and a product of programmed genome remodeling.

Methods

Nematode Sample Collection and Staging. *Ascaris* ovaries and testes were dissected from adult worms. *Ascaris* 1-cell embryos were collected from fresh ovaries by dissolving the tissue with two treatments: 0.5 N NaOH for 60 min at room temperature, followed by washing in cold PBS buffer, pH 2.0. Embryonation of *Ascaris* zygotes was performed in PBS, pH 2.0, at 30°C while shaking for 10 hr (1 cell), 48 hr (2-4 cells), 60 hr (4-8 cells), 5 days (32-64 cells), and 10 days (L1 larvae). Ovary, testes, and staged embryos were frozen in liquid nitrogen and stored at -80°C until use.

Collection of *P. univalens* zygotes and embryonation were performed as previously described (Simmons et al. 2024). Dissected zygotes were stored at 4°C. Embryonation was performed in PBS, pH 2.0, at 37°C while shaking for 0 hr (1 cell), 17 hr (2-4 cells), 24 hr (4-8 cells), 48 hr (100-500 cells), 60 hr (300-800 cells), or 72 hr (L1 larvae).

Hi-C Library Preparation. Fixation was performed using the Arima-HiC 2.0 kit standard input protocol for *Ascaris* ovaries and testis. For both *Ascaris* and *Parascaris* embryos, the low input protocol was used, with the following modification: cell membranes were disrupted by forcing cells through a small metal dounce in 5 mL of PBS + TC buffer (22% formaldehyde, 50 mM HEPES pH 8.0, 0.5 mM EGTA, 1 mM EDTA, 100 mM NaCl) kept on ice. Hi-C was performed using the Arima-HiC 2.0 kit according to the manufacturer's protocol (Arima, Cat#A410110).

Illumina libraries were constructed using the Swift Biosciences Accel-NGS 2S Plus DNA Library kit (Swift Cat# 21024) and the NEBNext Ultra II DNA Library Prep Kit (NEB). Libraries were amplified using the KAPA Library Amplification kit (Roche Cat# KK2620) according to the manufacturer's protocols. Sample concentrations were measured with a DNA Qubit (Invitrogen, Cat# Q33238), and library fragment sizes were confirmed using a TapeStation 4200 (Agilent).

Illumina libraries were sequenced using a NovaSeq 6000 paired-end reads (150 bp) to a depth of 16-60 folds.

Multi-omics Data Generation. The following datasets used for multi-omics analysis were previously published: ATAC-seq, RNA-seq, ChIP-seq for histone marks (H3K4me3, H3S10P, H3K36me2, H3K36me3, H3K9me3), and RNA Polymerase II (Wang et al. 2014; Kang et al. 2016; Wang et al. 2017; Wang et al. 2020).

Computational Analysis

Detailed bioinformatic methods are described in the Supplemental Material.

Computational Implementation and Artificial Intelligence Usage. Hi-C data processing and visualization were performed with custom Python and shell scripts (see Supplemental Code). Analyses were implemented in Python 3.9–3.10 (https://www.python.org) using NumPy v1.21.0–1.24.3 (Harris et al. 2020) for linear algebra operations, pandas v1.3.0–2.0.3 (McKinney 2010) for data manipulation, Matplotlib v3.5.0–3.7.1 (Hunter 2007) and seaborn v0.11.0 (Waskom 2021) for visualization, and SciPy v1.9.0 (Virtanen et al. 2020) for statistical tests. Claude Opus 4.6 and 4.8 (Anthropic; https://www.anthropic.com) assisted with script development and debugging and with refining technical descriptions for clarity and concision; all outputs were verified through manual inspection and comparison with published methods.

Data access

The Hi-C data for *Ascaris* and *Parascaris* generated in this study have been submitted to NCBI GEO repository (https://www.ncbi.nlm.nih.gov/geo/) under accession numbers GSE314626 and GSE315650, respectively. All data and scripts are also available at

https://github.com/jsimmo45/Nematode-3D-Genome-PDE. All newly generated custom Python and shell scripts required to reproduce the analyses are provided as Supplemental Code.

Competing interest statement

The authors declare no competing interests.

Acknowledgments

We thank Martin Neilsen for the *Parascaris* material and Bruce Bamber, Jeff Myers, and Routh Packing Co. for their support and hospitality in collecting *Ascaris* material. We thank the Wang lab members for helpful discussions. We also thank Brandon Estrem, Mariano Labrador, and Dick Davis for comments, edits, and critical reading of the manuscript. This work was supported by NIH grants to J. W. (R01AI155588 and R01GM151551) and R.P.M. (R35GM133557) and the University of Tennessee Knoxville Startup Funds to J.W.

Author contributions: J.R.S. and J.W. designed the project; J.R.S. made Hi-C libraries; J.R.S. improved the *Ascaris* genome assembly; J.R.S., T.X., and R.P.M. performed Hi-C data analysis; J.R.S. wrote the initial draft; J.W. wrote the manuscript; J.R.S., R.P.M., and J.W. reviewed and edited the manuscript; J.W. and R.P.M. provided supervision; and J.W. managed the project and provided funding.

References

Arnaiz O, Guerin F, Couloux A, Miro-Pina C, Pellerin G, Nekrasova I, Amselem J, Aury JM, Bhullar S, Frapporti A et al. 2026. The tiny germline chromosomes of Paramecium aurelia have an exceptionally high recombination rate and are capped by a new class of Helitrons. *BMC Biol* **24**.

Arnould C, Rocher V, Saur F, Bader AS, Muzzopappa F, Collins S, Lesage E, Le Bozec B, Puget N, Clouaire T et al. 2023. Chromatin compartmentalization regulates the response to DNA damage. *Nature* **623**: 183-192.

Azzaria M, McGhee JD. 1992. DNA synthesis in the early embryo of the nematode Ascaris suum. *Dev Biol* **152**: 89-93.

Bendich AJ, Rogers SO. 2025. The biological and evolutionary consequences of competition between DNA sequences that benefit the cell and DNA sequences that benefit themselves. *Nucleic Acids Res* **53**.

Betermier M, Klobutcher LA, Orias E. 2023. Programmed chromosome fragmentation in ciliated protozoa: multiple means to chromosome ends. *Microbiol Mol Biol Rev* doi:10.1128/mmbr.00184-22: e0018422.

Bian Q, Anderson EC, Yang Q, Meyer BJ. 2020. Histone H3K9 methylation promotes formation of genome compartments in Caenorhabditis elegans via chromosome compaction and perinuclear anchoring. *Proc Natl Acad Sci U S A* **117**: 11459-11470.

Blokhina YP, Nguyen AD, Draper BW, Burgess SM. 2019. The telomere bouquet is a hub where meiotic double-strand breaks, synapsis, and stable homolog juxtaposition are coordinated in the zebrafish, Danio rerio. *PLoS genetics* **15**: e1007730.

Bonev B, Mendelson Cohen N, Szabo Q, Fritsch L, Papadopoulos GL, Lubling Y, Xu X, Lv X, Hugnot JP, Tanay A et al. 2017. Multiscale 3D Genome Rewiring during Mouse Neural Development. *Cell* **171**: 557-572 e524.

Borodin P, Chen A, Forstmeier W, Fouche S, Malinovskaya L, Pei Y, Reifova R, Ruiz-Ruano FJ, Schlebusch SA, Sotelo-Munoz M et al. 2022. Mendelian nightmares: the germline-restricted chromosome of songbirds. *Chromosome Res* doi:10.1007/s10577-022-09688-3.

Chen J, Birchler JA, Houben A. 2022. The non-Mendelian behavior of plant B chromosomes. *Chromosome Res* **30**: 229-239.

Chiolo I, Altmeyer M, Legube G, Mekhail K. 2025. Nuclear and genome dynamics underlying DNA double-strand break repair. *Nature reviews Molecular cell biology* **26**: 538-557.

Chung G, Stevens L, Dai X, Hickey S, Kiontke K, Rughani P, Kieninger MR, Collins JC, Juul S, Piano F et al. 2026. Genome evolution in parthenogenetic nematodes shaped by chromosome rearrangements and introgression. *Genome Res* doi:10.1101/gr.281318.125.

Crane E, Bian Q, McCord RP, Lajoie BR, Wheeler BS, Ralston EJ, Uzawa S, Dekker J, Meyer BJ. 2015. Condensin-driven remodelling of X chromosome topology during dosage compensation. *Nature* **523**: 240-244.

Das M, Semple JI, Haemmerli A, Volodkina V, Scotton J, Gitchev T, Annan A, Campos J, Statzer C, Dakhovnik A et al. 2024. Condensin I folds the Caenorhabditis elegans genome. *Nat Genet* **56**: 1737-1749.

Dedukh D, Krasikova A. 2021. Delete and survive: strategies of programmed genetic material elimination in eukaryotes. *Biol Rev Camb Philos Soc* doi:10.1111/brv.12796.

Dekker J, Mirny LA. 2024. The chromosome folding problem and how cells solve it. *Cell* **187**: 6424-6450.

Drotos KHI, Zagoskin MV, Kess T, Gregory TR, Wyngaard GA. 2022. Throwing away DNA: programmed downsizing in somatic nuclei. *Trends Genet* **38**: 483-500.

Easton A, Gao S, Lawton SP, Bennuru S, Khan A, Dahlstrom E, Oliveira RG, Kepha S, Porcella SF, Webster J et al. 2020. Molecular evidence of hybridization between pig and human Ascaris indicates an interbred species complex infecting humans. *Elife* **9**.

Estrem B, Davis RE, Wang J. 2024. End resection and telomere healing of DNA double-strand breaks during nematode programmed DNA elimination. *Nucleic Acids Res* **52**: 8913-8929.

Estrem B, Wang J. 2023. Programmed DNA elimination in the parasitic nematode Ascaris. *PLoS Pathog* **19**: e1011087.

Feric M, Misteli T. 2021. Phase separation in genome organization across evolution. *Trends Cell Biol* **31**: 671-685.

Fujishiro S, Sasai M, Maeshima K. 2025. Chromatin domains in the cell: Phase separation and condensation. *Current opinion in structural biology* **91**: 103006.

Gassler J, Brandao HB, Imakaev M, Flyamer IM, Ladstatter S, Bickmore WA, Peters JM, Mirny LA, Tachibana K. 2017. A mechanism of cohesin-dependent loop extrusion organizes zygotic genome architecture. *Embo j* **36**: 3600-3618.

Gerstein MB Lu ZJ Van Nostrand EL Cheng C Arshinoff BI Liu T Yip KY Robilotto R Rechtsteiner A Ikegami K et al. 2010. Integrative analysis of the Caenorhabditis elegans genome by the modENCODE Project. *Science (New York, NY)* **330**: 1775-1787.

Giorgetti L, Lajoie BR, Carter AC, Attia M, Zhan Y, Xu J, Chen CJ, Kaplan N, Chang HY, Heard E et al. 2016. Structural organization of the inactive X chromosome in the mouse. *Nature* **535**: 575-579.

Giudice J, Jiang H. 2024. Splicing regulation through biomolecular condensates and membraneless organelles. *Nature reviews Molecular cell biology* **25**: 683-700.

Goloborodko A, Imakaev MV, Marko JF, Mirny L. 2016. Compaction and segregation of sister chromatids via active loop extrusion. *Elife* **5**.

Gonzalez de la Rosa PM, Thomson M, Trivedi U, Tracey A, Tandonnet S, Blaxter M. 2021. A telomere-to-telomere assembly of Oscheius tipulae and the evolution of rhabditid nematode chromosomes. *G3 (Bethesda)* **11**.

Grishanin A. 2014. Chromatin diminution in Copepoda (Crustacea): pattern, biological role and evolutionary aspects. *Comp Cytogenet* **8**: 1-10.

Hanlon VCT, Cagan A, Eves-van den Akker S. 2025. How and when organisms edit their own genomes. *Nat Genet* doi:10.1038/s41588-025-02230-1.

Harper L, Golubovskaya I, Cande WZ. 2004. A bouquet of chromosomes. *Journal of cell science* **117**: 4025-4032.

Harris CR, Millman KJ, van der Walt SJ, Gommers R, Virtanen P, Cournapeau D, Wieser E, Taylor J, Berg S, Smith NJ et al. 2020. Array programming with NumPy. *Nature* **585**: 357-362.

Herbette M, Ross L. 2023. Paternal genome elimination: patterns and mechanisms of drive and silencing. *Curr Opin Genet Dev* **81**: 102065.

Hu J, Zhang Y, Zhao L, Frock RL, Du Z, Meyers RM, Meng FL, Schatz DG, Alt FW. 2015. Chromosomal Loop Domains Direct the Recombination of Antigen Receptor Genes. *Cell* **163**: 947-959.

Hunter JD. 2007. Matplotlib: a 2D graphics environment. *Comput Sci Eng* **9**: 90-95.

Hyman AA, Weber CA, Julicher F. 2014. Liquid-liquid phase separation in biology. *Annu Rev Cell Dev Biol* **30**: 39-58.

Jack A, Kim Y, Strom AR, Lee DSW, Williams B, Schaub JM, Kellogg EH, Finkelstein IJ, Ferro LS, Yildiz A et al. 2022. Compartmentalization of telomeres through DNA-scaffolded phase separation. *Dev Cell* **57**: 277-290 e279.

Jash E, Csankovszki G. 2024. Chromatin Organization during C. elegans Early Development. *DNA* **4**: 64-83.

Kaaij LJT, van der Weide RH, Ketting RF, de Wit E. 2018. Systemic Loss and Gain of Chromatin Architecture throughout Zebrafish Development. *Cell reports* **24**: 1-10 e14.

Kang Y, Wang J, Neff A, Kratzer S, Kimura H, Davis RE. 2016. Differential Chromosomal Localization of Centromeric Histone CENP-A Contributes to Nematode Programmed DNA Elimination. *Cell Rep* doi:10.1016/j.celrep.2016.07.079.

Kim J, Jimenez DS, Ragipani B, Zhang B, Street LA, Kramer M, Albritton SE, Winterkorn LH, Morao AK, Ercan S. 2022. Condensin DC loads and spreads from recruitment sites to create loop-anchored TADs in C. elegans. *Elife* **11**.

Kim J, Wang H, Ercan S. 2025. Cohesin organizes 3D DNA contacts surrounding active enhancers in C. elegans. *Genome research* **35**: 1108-1123.

Kloc M, Kubiak JZ, Ghobrial RM. 2022. Natural genetic engineering: A programmed chromosome/DNA elimination. *Dev Biol* **486**: 15-25.

Lajoie BR, Dekker J, Kaplan N. 2015. The Hitchhiker's guide to Hi-C analysis: practical guidelines. *Methods (San Diego, Calif)* **72**: 65-75.

Li H, Playter C, Das P, McCord RP. 2024. Chromosome compartmentalization: causes, changes, consequences, and conundrums. *Trends Cell Biol* **34**: 707-727.

Luo Z, Hu T, Jiang H, Wang R, Xu Q, Zhang S, Cao J, Song X. 2020. Rearrangement of macronucleus chromosomes correspond to TAD-like structures of micronucleus chromosomes in Tetrahymena thermophila. *Genome research* **30**: 406-414.

MacQueen AJ, Phillips CM, Bhalla N, Weiser P, Villeneuve AM, Dernburg AF. 2005. Chromosome sites play dual roles to establish homologous synapsis during meiosis in C. elegans. *Cell* **123**: 1037-1050.

McCord RP, Kaplan N, Giorgetti L. 2020. Chromosome Conformation Capture and Beyond: Toward an Integrative View of Chromosome Structure and Function. *Mol Cell* **77**: 688-708.

McKinney W. 2010. Data structures for statistical computing in Python. In *Proceedings of the 9th Python in Science Conference*, doi:10.25080/Majora-92bf1922-00a (ed. S van der Walt, J Millman), pp. 56-61.

Minajigi A, Froberg J, Wei C, Sunwoo H, Kesner B, Colognori D, Lessing D, Payer B, Boukhali M, Haas W et al. 2015. A comprehensive Xist interactome reveals cohesin repulsion and an RNA-directed chromosome conformation. *Science (New York, NY)* **349**.

Mochizuki K. 2024. Programmed DNA elimination. *Curr Biol* **34**: R843-R847.

Muller F, Wicky C, Spicher A, Tobler H. 1991. New telomere formation after developmentally regulated chromosomal breakage during the process of chromatin diminution in Ascaris lumbricoides. *Cell* **67**: 815-822.

Muller LSM, Cosentino RO, Forstner KU, Guizetti J, Wedel C, Kaplan N, Janzen CJ, Arampatzi P, Vogel J, Steinbiss S et al. 2018. Genome organization and DNA accessibility control antigenic variation in trypanosomes. *Nature* **563**: 121-125.

Niedermaier J, Moritz KB. 2000. Organization and dynamics of satellite and telomere DNAs in Ascaris: implications for formation and programmed breakdown of compound chromosomes. *Chromosoma* **109**: 439-452.

Phillips CM, Dernburg AF. 2006. A family of zinc-finger proteins is required for chromosome-specific pairing and synapsis during meiosis in C. elegans. *Dev Cell* **11**: 817-829.

Pulupa J, McArthur NG, Stathi O, Wang M, Zazhytska M, Pirozzolo ID, Nayar A, Shapiro L, Lomvardas S. 2025. Solid phase transitions as a solution to the genome folding paradox. *Nature* **643**: 820-829.

Qing X, Zhang YM, Sun S, Ahmed M, Lo WS, Bert W, Holovachov O, Li H. 2025. Phylogenomic Insights into the Evolution and Origin of Nematoda. *Syst Biol* **74**: 349-358.

Rabuffo C, Schmidt MR, Yadav P, Tong P, Carloni R, Barcons-Simon A, Cosentino RO, Krebs S, Matthews KR, Allshire RC et al. 2024. Inter-chromosomal transcription hubs shape the 3D genome architecture of African trypanosomes. *Nat Commun* **15**: 10716.

Rajarajan P, Borrman T, Liao W, Schrode N, Flaherty E, Casino C, Powell S, Yashaswini C, LaMarca EA, Kassim B et al. 2018. Neuron-specific signatures in the chromosomal connectome associated with schizophrenia risk. *Science (New York, NY)* **362**.

Rzeszutek I, Maurer-Alcala XX, Nowacki M. 2020. Programmed genome rearrangements in ciliates. *Cell Mol Life Sci* doi:10.1007/s00018-020-03555-2.

Sabari BR, Dall'Agnese A, Young RA. 2020. Biomolecular Condensates in the Nucleus. *Trends Biochem Sci* **45**: 961-977.

Sanders JT, Freeman TF, Xu Y, Golloshi R, Stallard MA, Hill AM, San Martin R, Balajee AS, McCord RP. 2020. Radiation-induced DNA damage and repair effects on 3D genome organization. *Nat Commun* **11**: 6178.

Sawh AN, Mango SE. 2022. Chromosome organization in 4D: insights from C. elegans development. *Current opinion in genetics & development* **75**: 101939.

Sawh AN, Shafer MER, Su J-H, Zhuang X, Wang S, Mango SE. 2020. Lamina-Dependent Stretching and Unconventional Chromosome Compartments in Early C. elegans Embryos. *Molecular Cell* **78**: 96-111.e116.

Shin Y, Brangwynne CP. 2017. Liquid phase condensation in cell physiology and disease. *Science (New York, NY)* **357**.

Simmons JR, Estrem B, Zagoskin MV, Oldridge R, Zadegan SB, Wang J. 2024. Chromosome fusion and programmed DNA elimination shape karyotypes of nematodes. *Curr Biol* **34**: 2147-2161 e2145.

Smith JJ, Timoshevskiy VA, Saraceno C. 2021. Programmed DNA Elimination in Vertebrates. *Annu Rev Anim Biosci* **9**: 173-201.

Soranno A, Incicco JJ, De Bona P, Tomko EJ, Galburt EA, Holehouse AS, Galletto R. 2022. Shelterin Components Modulate Nucleic Acids Condensation and Phase Separation in the Context of Telomeric DNA. *J Mol Biol* **434**: 167685.

Spegg V, Panagopoulos A, Stout M, Krishnan A, Reginato G, Imhof R, Roschitzki B, Cejka P, Altmeyer M. 2023. Phase separation properties of RPA combine high-affinity ssDNA binding with dynamic condensate functions at telomeres. *Nature structural & molecular biology* **30**: 451-462.

Srinivasan J, Agbaga M, Terta V, Estrem B, Simmons JR, Oldridge R, Iftikhar M, West A, Lam H, Dockendorff TC et al. 2026. A sequence motif for DNA double-strand break and telomere healing during programmed DNA elimination. *bioRxiv* doi:10.64898/2026.03.06.709695: 2026.2003.2006.709695.

Stevens L, Sun S, Haruta N, Xiao L, Uwatoko N, Kieninger M, Sato K, Yoshida A, Absolon D, Collins J et al. 2025. Programmed DNA elimination was present in the last common ancestor of Caenorhabditis nematodes. *bioRxiv* doi:10.1101/2025.10.23.681605: 2025.2010.2023.681605.

Streit A, Wang J, Kang Y, Davis RE. 2016. Gene silencing and sex determination by programmed DNA elimination in parasitic nematodes. *Curr Opin Microbiol* **32**: 120-127.

Strom AR, Emelyanov AV, Mir M, Fyodorov DV, Darzacq X, Karpen GH. 2017. Phase separation drives heterochromatin domain formation. *Nature* **547**: 241-245.

Tandonnet S, Koutsovoulos GD, Adams S, Cloarec D, Parihar M, Blaxter ML, Pires-daSilva A. 2019. Chromosome-Wide Evolution and Sex Determination in the Three-Sexed Nematode Auanema rhodensis. *G3 (Bethesda)* **9**: 1211-1230.

Thadani R, Johnson N, Cooper JP. 2026. Chromosome Ends in Motion: Telomeres as Hazards and Hubs in Meiosis. *Cold Spring Harb Perspect Biol* **18**.

Tomita K, Cooper JP. 2007. The telomere bouquet controls the meiotic spindle. *Cell* **130**: 113-126.

Tsai JH, McKee BD. 2011. Homologous pairing and the role of pairing centers in meiosis. *Journal of cell science* **124**: 1955-1963.

Villano DJ, Prahlad M, Singhal A, Sanbonmatsu KY, Landweber LF. 2025. Widespread 3D genome reorganization precedes programmed DNA rearrangement in Oxytricha trifallax. *bioRxiv* doi:10.1101/2024.12.31.630814.

Virtanen P, Gommers R, Oliphant TE, Haberland M, Reddy T, Cournapeau D, Burovski E, Peterson P, Weckesser W, Bright J et al. 2020. SciPy 1.0: fundamental algorithms for scientific computing in Python. *Nat Methods* **17**: 261-272.

Wang J, Davis RE. 2014. Programmed DNA elimination in multicellular organisms. *Curr Opin Genet Dev* **27C**: 26-34.

Wang J, Davis RE. 2020. Ascaris. *Curr Biol* **30**: R423-R425.

Wang J, Gao S, Mostovoy Y, Kang Y, Zagoskin M, Sun Y, Zhang B, White LK, Easton A, Nutman TB et al. 2017. Comparative genome analysis of programmed DNA elimination in nematodes. *Genome Res* **27**: 2001-2014.

Wang J, Garrey J, Davis RE. 2014. Transcription in pronuclei and one- to four-cell embryos drives early development in a nematode. *Current biology : CB* **24**: 124-133.

Wang J, Mitreva M, Berriman M, Thorne A, Magrini V, Koutsovoulos G, Kumar S, Blaxter ML, Davis RE. 2012. Silencing of germline-expressed genes by DNA elimination in somatic cells. *Dev Cell* **23**: 1072-1080.

Wang J, Veronezi GMB, Kang Y, Zagoskin M, O'Toole ET, Davis RE. 2020. Comprehensive Chromosome End Remodeling during Programmed DNA Elimination. *Curr Biol* **30**: 3397–3413.

Waskom ML. 2021. seaborn: statistical data visualization. *J Open Source Softw* **6**: 3021.

Yoshida K, Rodelsperger C, Roseler W, Riebesell M, Sun S, Kikuchi T, Sommer RJ. 2023. Chromosome fusions repatterned recombination rate and facilitated reproductive isolation during Pristionchus nematode speciation. *Nature ecology & evolution* **7**: 424-439.

Zagelbaum J, Schooley A, Zhao J, Schrank BR, Callen E, Zha S, Gottesman ME, Nussenzweig A, Rabadan R, Dekker J et al. 2023. Multiscale reorganization of the genome following DNA damage facilitates chromosome translocations via nuclear actin polymerization. *Nature structural & molecular biology* **30**: 99-106.

Zagoskin M, Kang Y, Davis RE, Wang J. 2025. Argonautes and small RNAs associated with nematode programmed DNA elimination. *In bioRxiv* doi:10.1101/2025.10.23.684123.

Zagoskin MV, Wang J. 2021. Programmed DNA elimination: silencing genes and repetitive sequences in somatic cells. *Biochem Soc Trans* **49**: 1891-1903.

Zhang Y, McCord RP, Ho YJ, Lajoie BR, Hildebrand DG, Simon AC, Becker MS, Alt FW, Dekker J. 2012. Spatial organization of the mouse genome and its role in recurrent chromosomal translocations. *Cell* **148**: 908-921.

Zheng H, Xie W. 2019. The role of 3D genome organization in development and cell differentiation. *Nature reviews Molecular cell biology* **20**: 535-550.

Figure legends

Figure 1. CBRs interact with each other during *Ascaris* PDE. A. PDE breaks one germline chromosome into two somatic chromosomes. Chr 1, one of the 11 *Ascaris* germline chromosomes that has DNA eliminated in the middle of the chromosome, is illustrated. **B.** Hi-C maps of Chr 1 before (2-4 cells) and after (32-64 cells) PDE show the formation of the two somatic chromosomes following PDE. Intra-chromosomal (cis) interactions of Chr 1 at 10 kb resolution are shown; contact matrices were iteratively corrected (ICE method) and normalized to counts per million (CPM) within the displayed region. **C.** Hi-C heatmaps on *Ascaris* embryos from developmental stages before (2-4 cells, 48 hours), during (4-8 cells, 60 hours), and after (32-64 cells, 5 days) PDE are shown at 250 kb resolution, normalized to CPM genome-wide. In contrast to the single-chromosome maps in (B), these genome-wide maps include trans contacts. Thus, the color scale is set below the strong cis signal to show the weaker trans interactions between chromosome ends. Before and during PDE, Hi-C interactions are observed between the ends of chromosomes where CBRs reside. Notably, these interactions are not observed after PDE at the 32-64-cell stage. Black arrows indicate examples of interactions at the ends of the chromosomes, while green arrows denote examples of interactions at the middle of the chromosomes. **D.** Hi-C heatmaps of 400-kb flanking each CBR reveal strong interactions among terminal (upper left blocks) and internal CBRs (lower right blocks) before and during the PDE. Note that these two clusters of CBR interactions are not visible in the post-PDE stage (32-64-cell embryos). **E.** Zoomed-in portion of the Hi-C heatmap delineated in **Figure 1C** (2-4 cell, pre-PDE) showing interactions among CBRs from a selection of autosomes (boxed in Figure 1C, left panel). **F.** Principal components analysis of CBR interactions reveals two distinct clusters before and during PDE and one cluster after PDE. **G.** Examples of terminal and internal CBR interactions binned at 100 kb resolution.

Figure 2. CBR interactions are established during *Ascaris* germline development. Interactions between chromosome ends in *Ascaris* were present in the testis (**A**), ovary (**B**), and 1-cell zygote (**C**). Values were normalized using counts per million (CPM). Note the differences in the interactions as shown in dots (Ovary) vs. stripes (Testis and 1-cell zygote). Black and green arrows point to examples of the end-to-end and internal-to-internal interactions, respectively.

Figure 3. Interactions of CBR-adjacent regions are associated with PDE. A. CBR-adjacent regions have high interchromosomal interactions. The CBRs are highlighted in green with a vertical dashed line and designated as 0. The 500-kb retained side is to the left (in negative values), and the 100-kb eliminated side is to the right. *Trans* interaction frequencies surrounding 45 terminal CBRs are shown. Meta-profiles for all analyzed CBRs are displayed as mean (solid lines) ± one standard error of the mean (SEM, shaded areas). **B.** All chromosomes contribute to the CBR interactions observed in **Figure 3A**. The aggregated CBR *trans*-interaction for the testis was broken down by contributions from each chromosome (ordered and color-coded). **C.** CBR regions are highly insulated in the germline and early embryos through PDE. Insulation score is shown for each developmental stage for Chr 2. Less insulated regions (positive values) are shown in blue, more insulated regions (negative values) are shown in red. Eliminated regions are highlighted in red. **D.** The end eliminated regions are highly insulated. The whole genome is broken down by retained (blue), end eliminated (red), and internal eliminated (orange) regions. Insulation score values using a 100-kb window size are plotted for each developmental stage in a sliding window size of 5 kb. Post-PDE stages on the right are highlighted in red (note the lack of eliminated DNA data in post-PDE). Data points below -5 are shown as hollow circles. Statistical significance was calculated using a two-sided Mann-Whitney *U* test (*** $p<0.001$ and ** $p<0.01$). **E.** Interaction of CBRs at PDE foci in the nucleus. A 3D genome interaction model based on Hi-C maps. Shown are the dynamic changes of the CBRs

(red circles) in five chromosomes (five colored threads in their chromosome territories). PDE foci are shown in big yellow circles. Germline (old; green) and somatic (new; blue) telomeres are illustrated. Depicted are two CBRs interacting within a PDE focus (left, top), where a programmed DSB occurred. After DSB formation, new telomeres are added to the retained DNA, which then dissociates from the PDE foci (right, top). A newly formed CBR interaction is also shown (right, bottom). Meanwhile, internal CBRs interact among themselves apart from terminal CBRs, leading to drastic karyotype changes after elimination.

Figure 4. 3D chromosomal changes during embryogenesis and in response to programmed DSBs. A. Dynamic changes of insulation for retained ends of chromosomes. Insulation scores for 100 kb regions of retained DNA proximal to the end (47 sites; left) and middle (24 sites; right) of the chromosomes were determined. Shown are mean values with bars representing one standard error. Each dot represents the end of a somatic chromosome (or future somatic chromosome in pre-PDE stages). Statistical significance was calculated using a two-sided Mann-Whitney *U* test (*** $p<0.001$, ** $p<0.01$, and * $p<0.05$). Data points lower than -4 are shown as empty circles at the lower boundary. **B.** Changes in middle and long-range Hi-C interaction. Distance-decay curves for whole-genome Hi-C interaction data at different developmental stages. Normalized expected contact frequency (y-axis) is plotted against genomic distance (x-axis) on a log-log scale. **C.** Changes in the 3D interaction among chromosomes. Chromosomal cluster analysis was performed at each developmental stage. Pre-PDE genomes are shown with 24 chromosomes, while post-PDE genomes are shown with 36 chromosomes. Strong clusters emerge after PDE as observed in the group of sex chromosomes (top-left corners) in the 32-64-cell embryos and L1 larvae.

Figure 5. PDE splits chromosomes and causes 3D genome changes. A. Compartmentalization changes during *Ascaris* embryogenesis. Hi-C compartments were

902 determined by using the eigenvector 1 values through the developmental stage. Eliminated
903 regions are highlighted in light red (see Supplemental Fig. S7 for compartments for all
904 chromosomes). For Chr 1, weak compartmentalization between its two future somatic
905 derivatives is shown before PDE. Following PDE, the 3′ end of Chr 1a and the 5′ end of Chr 1b
906 occupy the same active compartment, while the 5′ end of Chr 1a and the 3′ end of Chr 1b
907 remain in the inactive compartment (see also Figure 5D). For Chr X1, after PDE split it into three
908 somatic chromosomes, the two terminal fragments occupy the same compartment while the
909 central fragment is segregated away (see also Figure 5D). **B.** Multiomics analysis confirms the
910 defined compartments. Active chromatin marks are enriched in A compartments, while a
911 heterochromatin mark is enriched in B compartments. Each point represents a 100 kb genomic
912 region. A two-sided Mann-Whitney *U* test was performed to calculate the statistical significance
913 for each comparison (*** $p<0.001$, ** $p<0.01$, and * $p<0.05$). **C.** Dynamics of compartment
914 interactions through development. A/B compartment interactions are shown using saddle plots.
915 Genomic bins are sorted by PC1 value and binned into 20 quantiles (both axes). Contact
916 enrichment within each bin pair is displayed (red = high; blue = low). Dashed yellow lines mark
917 the A/B boundary (PC1 = 0). **D**. Model of chromosomal rearrangements following PDE. The
918 germline chromosomes are not strongly compartmentalized in the early embryos. After PDE, the
919 resulting somatic chromosomes reorganize their compartments. The two chromosomes were
920 modeled based on data from Figure 5A.
921
922 **Figure 6. Transient cis interactions between cognate CBRs during *Parascaris* PDE. A.** Hi-
923 C contact map of the *Parascaris* embryos before, during, and after PDE. The germline
924 karyotype for female is XX and male is XY, where the Y Chromosome lacks the sex
925 chromosome region (yellow box). The apparent interaction between the two boundaries of the
926 sex chromosome region arises because the sequences at the two boundaries are juxtaposed in
927 the Y Chromosome of the males. Thus, in a population of embryos with mixed sexes, ~25% of

928 the chromosomes lack this region (Simmons et al. 2024). The map covers the ~240 Mb
929 assembled genome and the ~2.2 Gb of repetitive heterochromatic arms which are eliminated
930 (not shown). The shown eliminated regions and all CBRs are internal and are ~1 Gb away from
931 the chromosome ends, so their interactions are unlikely affected by germline telomere
932 interactions. **B.** Pairwise CBR interactions during *Parascaris* PDE. Observed/expected contact
933 ratio map for the same stages as in **Figure 6A**. Strong focal interactions are visible between
934 cognate CBR pairs. **C.** Zoomed-in portion of the Hi-C heatmap delineated in **Figure 6B** (2-4 cell,
935 during-PDE) showing interactions among CBRs from a selection of autosomes. Black arrows
936 indicate interactions between cognate CBRs; green arrows indicate interactions between non-
937 cognate CBRs. **D.** Exemplary dynamic CBR interactions throughout PDE. Interaction
938 frequencies across ChrX 89–101 Mb are shown before, during and after PDE. Black arrows
939 mark the cognate CBR interactions. **E.** *Parascaris* CBRs spatially demarcate the retained and
940 eliminated DNA. Normalized contact frequency between cognate CBRs. Hi-C interactions for
941 500 kb of retained DNA (left) and 100 kb of eliminated DNA (right) flanking all 72 CBRs (vertical
942 dashed line) were plotted. The interaction peaks immediately at the break during PDE and is
943 absent before and after. Note the interaction frequency falls to zero post PDE (4-8 cells) due to
944 the loss of the eliminated DNA. **F.** A model for CBR interactions during *Parascaris* PDE.
945 Germline Hi-C interactions among future somatic chromosomes are shown with red-orange-
946 yellow-white scale triangles, while interactions among eliminated regions are outlined with
947 dashed lines (not to scale). Green spots represent interactions between cognate CBR pairs
948 near the ends of each future somatic chromosome. Note the resemblance of the pre-PDE
949 chromosome structure to the “beads-on-a-string” model (Niedermaier and Moritz 2000).
950
951 **Figure 7. Chromosomal compartments are conserved between *Ascaris* and *Parascaris*. A.**
952 Eigenvector 1 values show conserved compartmentalization between *Ascaris* (red) and
953 *Parascaris* (blue) in L1 larvae stages (after PDE). Positive values represent A (active)

compartments and negative values represent B (inactive) compartments. Eliminated regions are shown with light red highlights. The chromosomes are ordered based on their positions along the length of the single germline chromosome of *Parascaris*, with the coordinates shown at the bottom in Mb. Matching somatic chromosomes in *Ascaris* that are flipped on the x-axis (i.e., genome coordinates) are labeled with (R). **B.** PDE converts distinct germline karyotypes in *Ascaris* and *Parascaris* into identical somatic karyotypes with identical somatic 3D genome organization. See text in the Discussion section for a description of this summary figure.

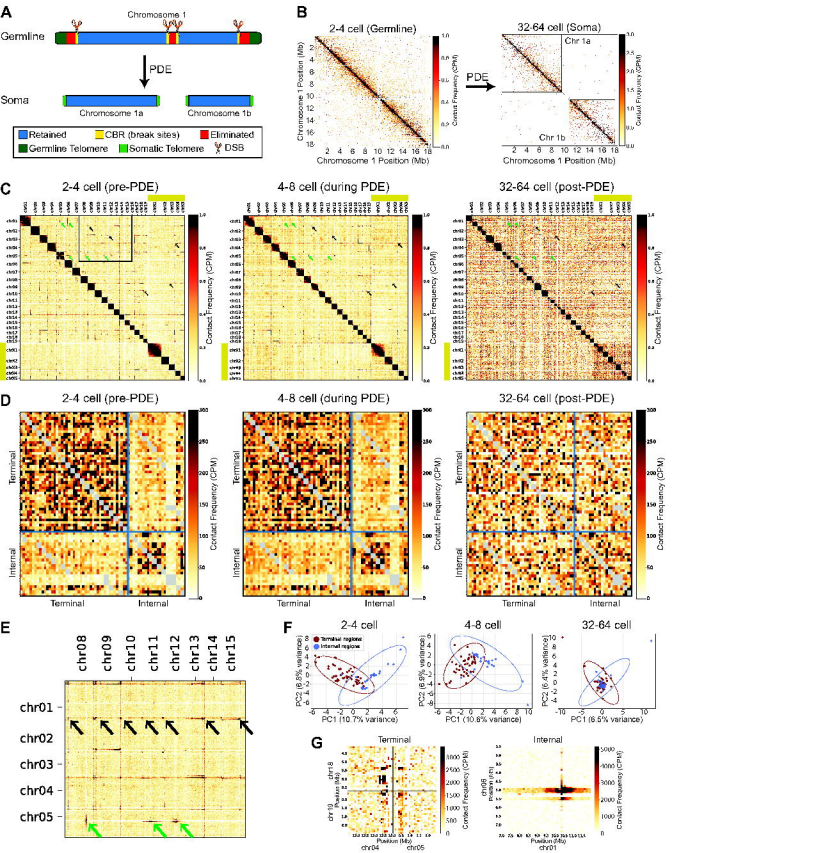
A
Chromosome 1
Germline
PDE
Soma
Chromosome 1a
Chromosome 1b
Retained
CBR (break sites)
Eliminated
Germline Telomere
Somatic Telomere
DSB
B
2-4 cell (Germline)
32-64 cell (Soma)
PDE
Chr 1a
Chr 1b
Chromosome 1 Position (Mb)
Contact Frequency (CPM)
C
2-4 cell (pre-PDE)
4-8 cell (during PDE)
32-64 cell (post-PDE)
Contact Frequency (CPM)
D
2-4 cell (pre-PDE)
4-8 cell (during PDE)
32-64 cell (post-PDE)
Terminal
Internal
Contact Frequency (CPM)
E
chr08
chr09
chr10
chr11
chr12
chr13
chr14
chr15
chr01
chr02
chr03
chr04
chr05
F
2-4 cell
4-8 cell
32-64 cell
Terminal regions
Internal regions
PC1 (10.7% variance)
PC1 (10.8% variance)
PC1 (8.5% variance)
PC2 (8.8% variance)
PC2 (8.8% variance)
PC2 (6.4% variance)
G
Terminal
Internal
chr08
chr09
chr10
chr04
chr05
chr01
Position (Mb)
Contact Frequency (CPM)

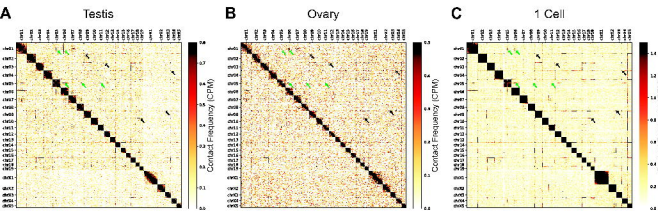
A
Testis
Contact Frequency (CPM)
B
Ovary
Contact Frequency (CPM)
C
1 Cell
Contact Frequency (CPM)

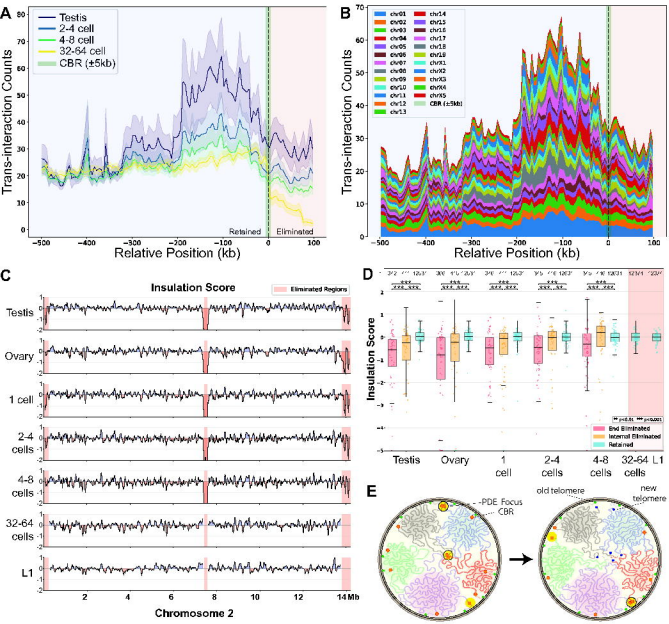
A
Testis
2-4 cell
4-8 cell
32-64 cell
CBR (±5kb)
Trans-interaction Counts
Retained
Eliminated
Relative Position (kb)
B
Trans-interaction Counts
Relative Position (kb)
C
Insulation Score
Eliminated Regions
Testis
Ovary
1 cell
2-4 cells
4-8 cells
32-64 cells
L1
Chromosome 2
D
Insulation Score
Testis
Ovary
1 cell
2-4 cells
4-8 cells
32-64 cells
L1
End Eliminated
Internal Eliminated
Retained
E
PDE Focus
CBR
old telomere
new telomere

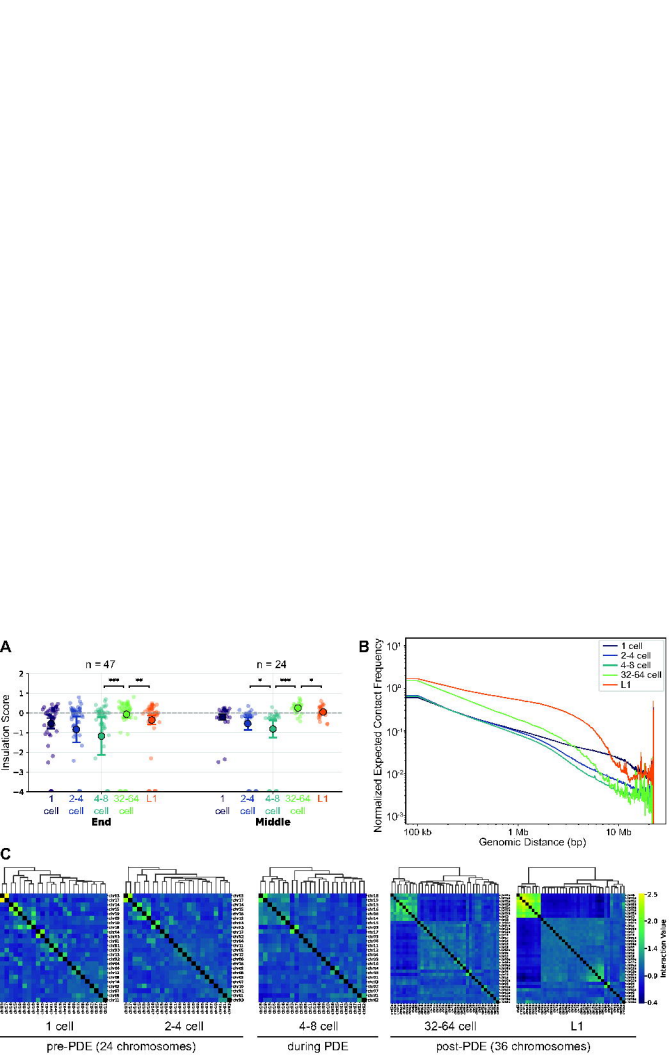
A
n = 47
n = 24
***
**
*
***
*
Insulation Score
2
1
0
−1
−2
−3
−4
1 cell
2-4 cell
4-8 cell
32-64 cell
L1
End
Middle
B
1 cell
2-4 cell
4-8 cell
32-64 cell
L1
Normalized Expected Contact Frequency
10^{0}
10^{-1}
10^{-2}
10^{-3}
100 kb
1 Mb
10 Mb
Genomic Distance (bp)
C
2.5
2.0
1.4
0.9
0.4
Interaction Value
1 cell
2-4 cell
4-8 cell
32-64 cell
L1
pre-PDE (24 chromosomes)
during PDE
post-PDE (36 chromosomes)

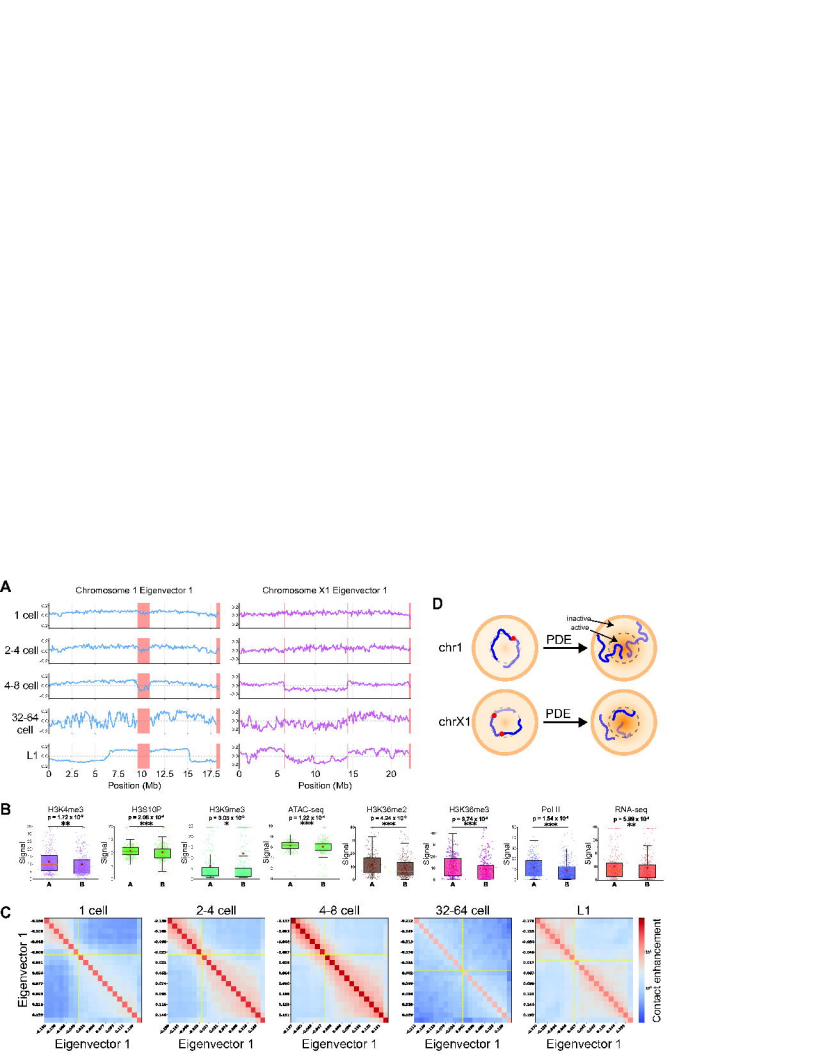
A
Chromosome 1 Eigenvector 1
Chromosome X1 Eigenvector 1
1 cell
2-4 cell
4-8 cell
32-64 cell
L1
Position (Mb)
Position (Mb)
D
chr1
chrX1
PDE
PDE
inactive
active
B
H3K4me3
H3S10P
H3K9me3
ATAC-seq
H3K36me2
H3K36me3
Pol II
RNA-seq
Signal
A
B
C
1 cell
2-4 cell
4-8 cell
32-64 cell
L1
Eigenvector 1
Eigenvector 1
Contact enhancement

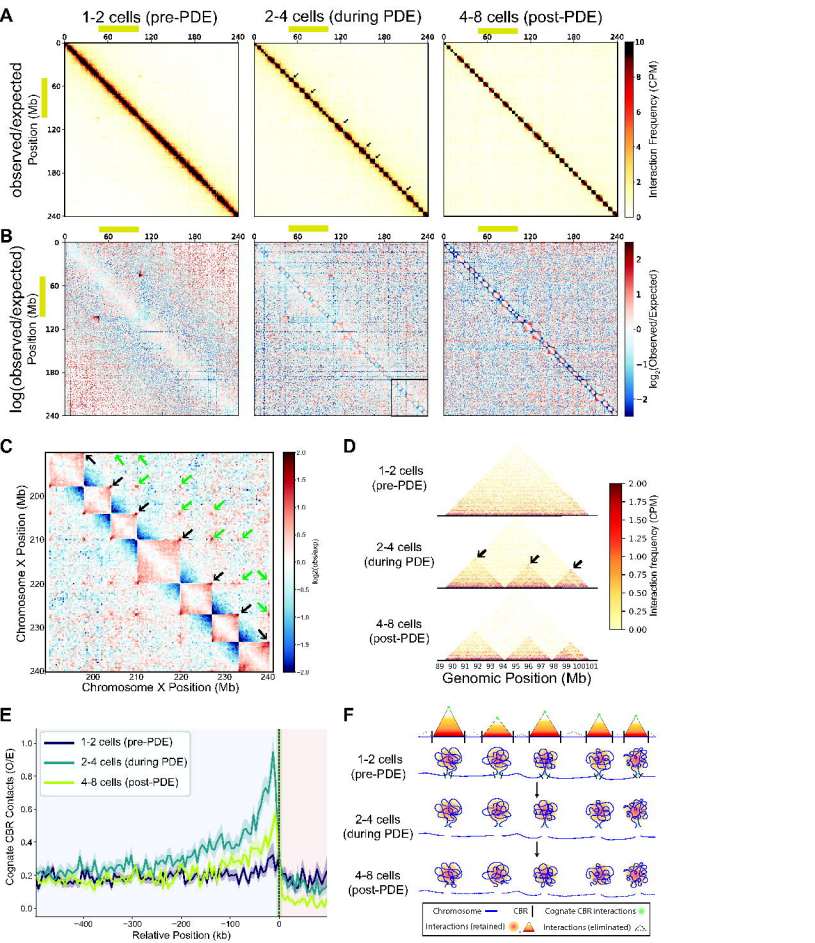
A
1-2 cells (pre-PDE)
2-4 cells (during PDE)
4-8 cells (post-PDE)
observed/expected
Position (Mb)
Interaction Frequency (CPM)
B
log(observed/expected)
Position (Mb)
log2(Observed/Expected)
C
Chromosome X Position (Mb)
Chromosome X Position (Mb)
log2(O/Exp)
D
1-2 cells
(pre-PDE)
2-4 cells
(during PDE)
4-8 cells
(post-PDE)
Interaction frequency (CPM)
Genomic Position (Mb)
E
1-2 cells (pre-PDE)
2-4 cells (during PDE)
4-8 cells (post-PDE)
Cognate CBR Contacts (O/E)
Relative Position (kb)
F
1-2 cells
(pre-PDE)
2-4 cells
(during PDE)
4-8 cells
(post-PDE)
Chromosome
CBR
Cognate CBR interactions
Interactions (retained)
Interactions (eliminated)

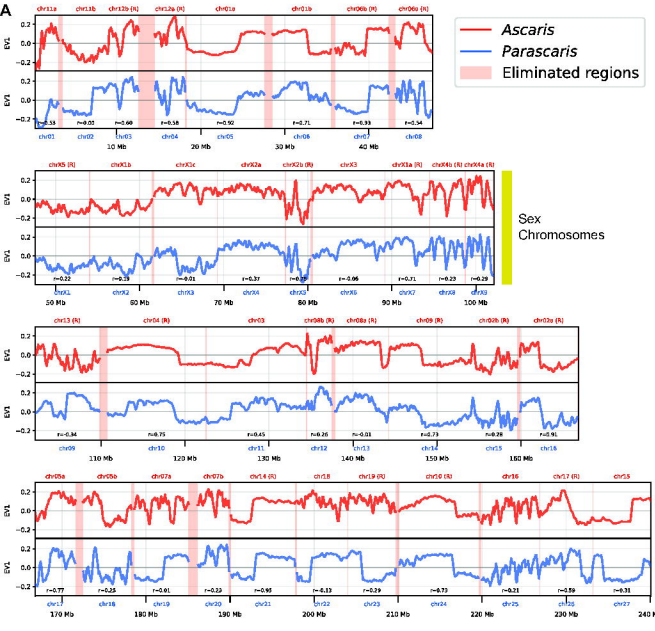
A
Ascaris
Parascaris
Eliminated regions
EVL
Sex Chromosomes
10 Mb
20 Mb
30 Mb
40 Mb
50 Mb
60 Mb
70 Mb
80 Mb
90 Mb
100 Mb
110 Mb
120 Mb
130 Mb
140 Mb
150 Mb
160 Mb
170 Mb
180 Mb
190 Mb
200 Mb
210 Mb
220 Mb
230 Mb
240 Mb

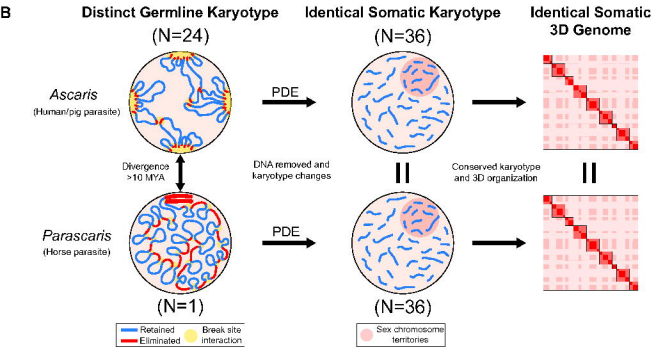
B
Distinct Germline Karyotype
Identical Somatic Karyotype
Identical Somatic 3D Genome
(N=24)
(N=36)
Ascaris
(Human/pig parasite)
PDE
Divergence >10 MYA
DNA removed and karyotype changes
Conserved karyotype and 3D organization
Parascaris
(Horse parasite)
PDE
(N=1)
(N=36)
Retained
Eliminated
Break site interaction
Sex chromosome territories